Wideband DS-CDMA for Next-Generation Mobile Communications Systems

Fumiyuki Adachi, Mamoru Sawahashi, and Hirohito Suda
NTT Mobile Communications Network Inc.

ABSTRACT Wideband wireless access based on direct sequence code division multiple access aimed at third-generation mobile communications systems is reviewed. W-CDMA is designed to flexibly offer wideband services which cannot be provided by present cellular systems, with various data rates as high as 2 Mb/s. The important concept of W-CDMA is the introduction of intercell asynchronous operation and the pilot channel associated with individual data channels. Intercell asynchronous operation facilitates continuous system deployment from outdoors to indoors. Other technical features of W-CDMA include fast cell search under intercell asynchronous operation, fast transmit power control, coherent spreading code tracking, a coherent Rake receiver, orthogonal multispreading factor forward link, and variable-rate transmission with blind rate detection. The introduction of the data-channel-associated pilot channel allows W-CDMA to support interference cancellation and adaptive antenna array techniques that can significantly increase the link capacity and coverage. This article presents radio link performance evaluated by computer simulation. Field experiment radio link performance results are also presented.

Recently, mobile communications services are penetrating into our society at an explosive growth rate. All of the current second-generation cellular communications systems (e.g., PDC/GSM/IS54 and IS95) have adopted digital technology. However, the major services they provide are limited to basic services, such as voice, facsimile, and low-bit-rate (far less than 64 kb/s) data. We are now approaching the 21st century, when demands for a variety of wideband services such as high-speed Internet access and video/high-quality image transmission, will continue to increase. The third-generation mobile communication systems, called International Mobile Telecommunications-2000 (IMT-2000) in the International Telecommunication Union (ITU) [1], must be designed to support wideband services at data rates as high as 2 Mb/s, with the same quality as fixed networks. Direct sequence code-division multiple access (DS-CDMA) technology [2] is attractive for wireless access because of its numerous advantages over time-division multiple access (TDMA) and frequency-division multiple access (FDMA), including soft handoff (or site diversity), exploitation of multipath fading through Rake combining, and direct capacity increase by the use of cell sectorization. However, the current IS-95 is based on narrowband DS-CDMA technology optimized for basic services. To realize true IMT-2000 systems, a new wideband wireless access technology incorporating as many recent technology developments as possible is necessary. The most promising candidate, wideband DS-CDMA (W-CDMA), is being developed throughout the world [3, 4].

In January 1998, the European Telecommunications Standards Institute (ETSI) decided to adopt W-CDMA technology for frequency-division duplex (FDD) bands. In Japan, the Association of Radio Industries and Businesses (ARIB), the standardization body of the radio sector, is now developing a W-CDMA air interface standard. ETSI W-CDMA and ARIB W-CDMA are based on a common design concept. It is strongly expected that they will eventually become a global standard.

This article is a comprehensive introduction to the W-CDMA technology that the authors have developed so far with the aim of IMT-2000. Our early version of W-CDMA [3] became the foundation of ARIB W-CDMA. However, our more recent research results on wireless transmission techniques have been incorporated into present W-CDMA technology to improve performance and flexibility. Note that the W-CDMA technology presented in this article does not necessarily reflect the very latest standardization works in progress within ETSI and ARIB. The following section overviews the W-CDMA technology and discusses the link performance. A series of field experiments on W-CDMA link performance using the 2 GHz carrier frequency band reserved for IMT-2000 systems was conducted in Tokyo. 1.92 Mb/s data transmission was also examined. The field experiment results are presented. The introduction of interference cancellation and adaptive antenna array techniques can reduce multi-access interference (MAI), and thus increase link capacity. W-CDMA is designed to support them. We then briefly introduce interference cancellation and adaptive antenna array techniques. Recently, channel coding using turbo codes is attracting much attention. This technique is also introduced.

W-CDMA Technology

The Design Concept

The important concept of W-CDMA is introduction of intercell asynchronous operation and the pilot channel associated with each data channel. The pilot channel makes coherent detection possible on the reverse link. Furthermore, it makes it possible to adopt interference cancellation and adaptive antenna array techniques at a later date. It is well known that cell sectorization can increase link capacity significantly; the adaptive antenna array is viewed as adaptive cell sectorization and is very attractive. Other technical features of W-CDMA are summarized below:

- Fast cell search under intercell *asynchronous* operation
- Coherent spreading-code tracking
- Fast transmit power control (TPC) on both reverse (mobile-to-cell-site) and forward (cell-site-to-mobile) links
- Coherent Rake reception on both links

0163-6804/98/$10.00 © 1998 IEEE

- Orthogonal multiple spreading factors (SFs) in the forward link
- Variable-rate transmission with blind rate detection

The radio link parameters are listed in Table 1. A simplified structure of the transmission frame is depicted in Fig. 1. The 10-ms data frame consists of 16 slots with pilot symbols at the beginning of each slot, followed by fast TPC command and coded data. The binary data sequence of the 10 ms frame to be transmitted is first channel-coded and then block bit-interleaved for mapping onto the 16 slots. Unless noted, rate-1/3 convolutional coding is assumed in this article; turbo coding is introduced later in this article. On the forward link (base-to-mobile), the interleaved, coded data sequence of one frame is transformed into a quaternary phase shift keying (QPSK)-modulated symbol sequence and is time-multiplexed every 0.625 ms with N_p pilot symbols and TPC command. The QPSK symbol sequence is QPSK-spread — orthogonal binary phase shift keying (BPSK) spreading and QPSK scrambling are applied. On the reverse link (mobile-to-base), BPSK data modulation is applied and the pilot channel is I/Q-multiplexed before QPSK spreading. (In this article, the time-multiplexed pilot channel only is considered.) Finally, the spread signal is power amplified (fast TPC is applied) before transmission in the 2 GHz carrier frequency band. The received multipath signal is matched-filtered — a matched filter (MF) can be implemented using a bank of synchronous correlators — and resolved into multiple replicas of the transmitted QPSK symbol sequence that had propagated along paths with different time delays. Resolved symbol sequences are coherently Rake combined. The Rake combiner output sample sequence is transformed into a soft-decision data sample sequence corresponding to the channel-coded binary data sequence and deinterleaved for succeeding soft-decision Viterbi decoding to recover the transmitted data. For fast TPC operation, the Rake combiner output signal-to-interference (plus background noise) ratio (SIR) is measured and compared with the target SIR to generate the TPC command which is transmitted every 0.625 ms to the mobile (cell site) via the forward link (reverse link) to raise or lower the transmit power. At the cell site receiver, two spatially separated antennas are used to reduce the mobile transmit power.

How the pilot channel is multiplexed with individual data channels is closely related to the variable-rate data transmission scheme adopted. The terms *multirate* and *variable-rate* mean that the average data rates of different users are different and that the data rate of a particular user changes either time to time or frame by frame, respectively. In this article we focus on the description of the time-multiplexed pilot channel structure and slotted variable-rate transmission with blind rate detection. (Later we will introduce continuous variable rate transmission with blind rate detection.) However, the parallel pilot channel is also attractive since it avoids bursty transmission which may cause unnecessary problems from electromagnetic compatibility (EMC). The I/Q multiplexed pilot structure may be suitable for the reverse link (mobile transmission) application. On the other hand, the time-multiplexed pilot channel structure and slotted variable-rate transmission with blind rate detection may be suitable for the forward link (mobile reception) because of the simplicity of mobile receiver processing.

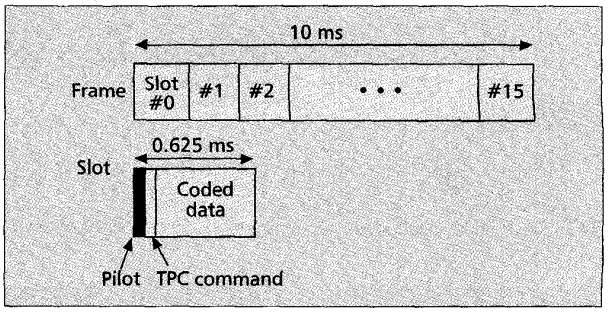

■ **Figure 1.** *Frame structure using time-multiplexed pilot.*

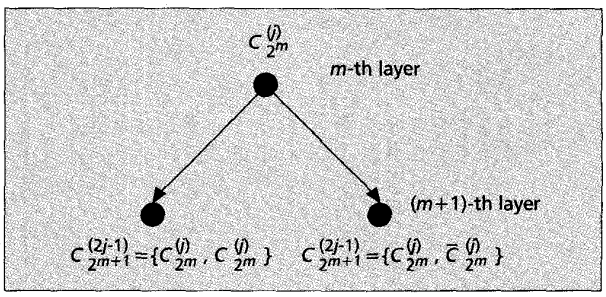

■ **Figure 2.** *Code generation (see Fig. 8 of Ref. [16]).*

Bandwidth (MHz)		1.25/5/10/20
Chip rate (Mc/s)		1.024/4.096/8.192/16.384
Spreading Code	Short Scramble	Tree-structured orthogonal multi-SF codes Pseudo noise codes
Modem	Spreading Data	QPSK Coherent QPSK/BPSK (forward/reverse links)
Channel coding		Voice: convolutional (R = 1/3, K = 9) Data: concatenation of convolutional+RS
Diversity		Rake+antenna
Power control		SIR-based fast TPC
Inter-cell operation		Async. (sync. possible)

■ **Table 1.** *Radio link parameters.*

Fast Cell Search Under Intercell Asynchronous Operation

It is easier to realize continuous system deployment, from outdoors to indoors, with an intercell *asynchronous* system than with an intercell synchronous system. This is because the former does not require any external timing source such as Global Positioning System (GPS) as used in IS-95. Unlike IS-95-based systems, a different cell site is assigned a unique scramble code on its forward link. In general, the use of different scramble codes at different cell sites increases the cell search time.

A fast cell search algorithm is described in [5]. The forward link control channels of all cell sites reuse the same short spreading code (e.g., $C_{64}^{(1)}$ from the set of orthogonal multi-SF codes), and the scramble code sequence (whose length is the same as the data frame length) is periodically masked over one symbol duration so that the $C_{64}^{(1)}$-code appears periodically during the scramble code period. During the masking period, the group identification (GI) code indicating the code group to which the scramble code of each cell site belongs is transmitted in parallel. The GI code can be chosen from the set of orthogonal multi-SF codes, for example,

$$\left\{C_{64}^{(j)}\right\}_{j=2}^{64}$$

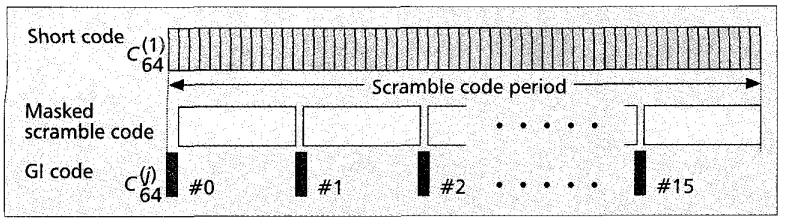

■ **Figure 3.** *Scramble code masking timing and GI code transmission.*

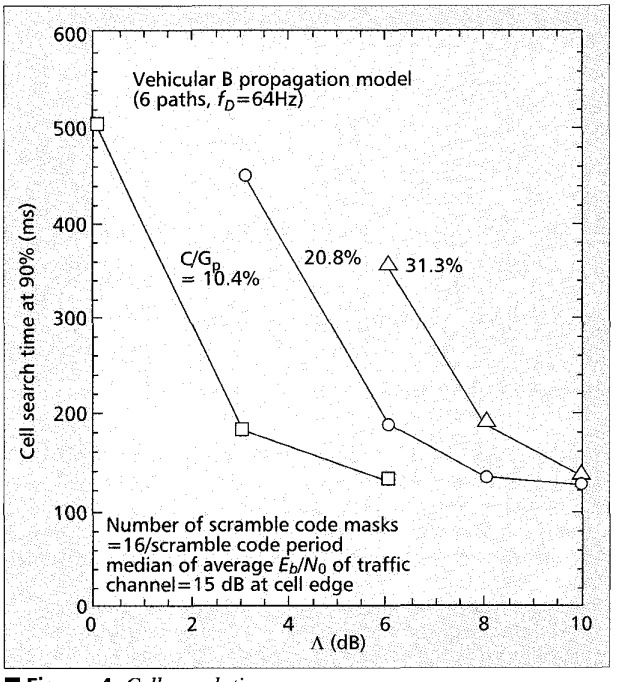

■ **Figure 4.** *Cell search time.*

The scramble code masking timing and GI code transmission are illustrated in Fig. 3. The three-step cell search algorithm involves:

1 Detecting the scramble code mask timing of the best cell site (determined using the least sum of propagation path loss plus shadowing) by the $C_{64}^{(1)}$ code MF
2 Identifying the scramble code group by taking the cross-correlation between the received signal and all GI code candidates
3 Searching for the scramble code by cross-correlating the received signal with all scramble code candidates belonging to the identified GI code

The speed of cell search accomplished in this way is plotted in Fig. 4 as a function of the transmit power ratio Λ of control channel over data channel. The number C of users normalized by processing gain G_p (defined as the chip-rate-to-information-bit-rate ratio, which is given by G_p = 64 x 3 x 0.5 = 96 in this simulation) is a parameter. The simulation parameters were as follows: a total of 32 x 16 scramble codes (32 code groups), a 64 ksymbols/s control channel with the chip rate of 4.096 Mchips/s, 16 masking events per scramble code period, and 16 parallel correlators in the third step. The simulation assumed the coverage area of 19 hexagonal omni-cells, the ITU — Radiocommunication Sector (ITU-R) Vehicular B propagation model having six Rayleigh faded paths (the maximum Doppler frequency f_D = 64 Hz), the distance-dependent path loss of decay factor 3.8, and log-normal shadowing of standard deviation 10 dB. The median of the local average signal-energy-to-background-noise power spectrum density ratio E_b/N_0 of each data channel was 15 dB at the cell edge (note that the average signal-energy-to-interference plus background noise power spectrum density ratio E_b/I_0 at the cell edge is much less than the average E_b/N_0 due to other-cell MAI). If the scramble code belonging to the cell site having the sum of path loss and shadowing within 3 dB from the best cell site is searched, cell search is declared to be successful; otherwise, it failed. Even for heavy traffic loads such as C/G_p = 20.8 percent (if voice activity detection is applied, this corresponds to C/G_p > 40 percent), the cell search can be accomplished within about 450 ms at 90 percent of locations even at Λ = 3 dB. It should be pointed out that although the periodic destruction of orthogonality gives rise to interference on data channels, the performance degradation is negligible due to the effects of channel coding and bit interleaving.

During soft handoff, a mobile must find the best cell sites to which it should communicate simultaneously. Since the number of candidate cell sites is at most 3–4 cells and the mobile can be informed of them from the current cell site, the cell search time for soft handoff can be greatly reduced.

Coherent Tracking of Spreading Code

The noncoherent delay-locked tracking loop (DLL) is the most popular and well-developed technique. It suffers from tracking jitter due to the noise enhancement arising from the square-law detector (squaring loss). The coherent DLL overcomes this problem and improves the transmission performance. However, it requires accurate channel estimation in the receiver, which is generally difficult to do in fast fading. Fortunately, the chip synchronization process can take advantage of the pilot channel. The block diagram of the coherent DLL is shown in Fig. 5. The received spread signal $r(t)$ is cross-correlated with advanced and retarded replicas, $c(t - \hat{\tau} + \Delta)$ and $c(t - \hat{\tau} - \Delta)$, of the spreading code sequence, where Δ is the chip timing offset. The integrate-and-dump (I & D) filter outputs of two DLL branches are combined to obtain the chip timing error signal ε_i, which contains the data modulation and the carrier phase and amplitude variations due to fading. The chip timing error signal ε_i is reverse-modulated by feeding back the i-th detected symbol $\hat{d}_i$ and is multiplied by the complex conjugate of the estimated fading envelope ξ_i to obtain the phase corrected chip timing error $\hat{\varepsilon}_i$. The channel estimation is performed by using pilot symbols of succeeding

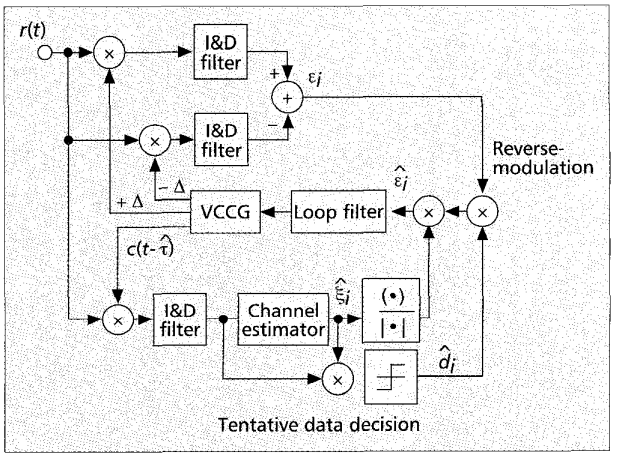

■ **Figure 5.** *Coherent DLL.*

two slots. The resulting chip timing error $\hat{\varepsilon}_i$ is smoothed by the loop filter to control the voltage controlled code generator (VCCG). By using only the in-phase component of the filtered chip timing error, the impact of the MAI and background noise can be decreased by about 3dB compared to noncoherent DLL. It was demonstrated that coherent DLL reduces the rms tracking jitter by almost one order of magnitude, and the required E_b/N_0 at the average bit error rate (BER) of 10^{-2} is improved by about 1–1.4dB under Rayleigh fading environments.

FAST TPC

DS-CDMA links are interference-limited. Fast TPC based on the measurement of SIR can always minimize the transmit power according to the traffic load and thus, interference to other users in the other cells can be reduced; thereby increasing the link capacity. SIR measurement is done after Rake combining. The frame structure using time-multiplexed pilots well supports SIR measurement. Both pilot and data symbols are used to measure instantaneous received signal power, but only pilot symbols are used to measure instantaneous interference plus background noise power (followed by averaging using a first order filter). The channel estimation is first performed using the pilot symbols. The MF output signal $r_l(n, k)$ at the n-th symbol position of k-th slot associated with the l-th propagation path is weighted by the complex conjugate of channel estimate $\tilde{\xi}_l(k)$ to remove the fading-induced random phase. Assuming that the number of Rake fingers is L, the Rake combiner output is represented as

$$\tilde{r}(n,k) = \sum_{l=0}^{L-1} r_l(n,k)\tilde{\xi}_l^*(k), \quad 0 \le n \le N_{\text{slot}} - 1,$$

where $\tilde{\xi}_l(k)$ is the simple average of N_p pilot symbols belonging to the k-th slot. $\tilde{r}(n, k)$ is used for measuring the SIR $\tilde{\lambda}(k)$ which is defined as $\tilde{\lambda}(k) = \tilde{S}(k)/\tilde{I}(k)$, where $\tilde{S}(k)$ and $\tilde{I}(k)$ are the instantaneous signal power and the average interference power, respectively. The Rake combiner output is reverse-modulated by the tentative symbol decision and accumulated to reduce the effect of MAI plus background noise, followed by the square operation to obtain the instantaneous signal power. The instantaneous MAI plus background noise power $\tilde{I}(k)$ is obtained from the squared error of the received pilot samples and then, averaged using a first order filter with forgetting factor $\alpha < 1$. $\tilde{S}(k)$ and $\tilde{I}(k)$ are computed from

$$\begin{aligned}
\tilde{S}(k) &= \left| \frac{1}{N_m} \left(\sum_{n=0}^{N_p-1} \tilde{r}(n,k) + \sum_{n=Np}^{N_m-1} \tilde{r}(n,k)\exp - j\tilde{\phi}(n,k) \right) \right|^2 \\
\tilde{\phi}(n,k) &= \max_{\phi \in \{m\pi/2; m=0-3\}} \text{Re}[\tilde{r}(n,k)\exp - j\phi] \qquad (1) \\
\tilde{I}(k) &= \alpha\tilde{I}(k-1) + (1-\alpha)\tilde{I}(k), \quad \tilde{I}(k) \\
&= \frac{1}{N_p} \sum_{n=0}^{N_p-1} \left| \tilde{r}(n,k) - \sum_{l=0}^{L-1} \tilde{\xi}_l(k) \right|^2
\end{aligned}$$

When D-branch antenna diversity is used, L should be replaced $D \cdot L$. Typical values of N_p, N_m, and α are $N_p = 4$, $N_m = 10$ (for slot length $N_{\text{slot}} = 40$), and $\alpha = 0.999$. This allows one-slot TPC delay. The measured SIR is compared with the target value λ_0 to generate the TPC command to raise or lower the transmit power by 1 dB every 0.625 ms. The TPC target value is determined according to the required communication quality.

The above fast TPC is applied to both reverse and forward links. The forward link is synchronous, and all forward link channels are spread using orthogonal multi-SF codes (this is called orthogonal spreading). Orthogonal spreading with Rake combining provides larger capacity than random spreading, even in frequency-selective fading channels, because of the absence of MAI within each path. In a cellular system, however, as the user moves away from the base station, the received signal power reduces due to increasing distance-dependent path loss; thus, the effects of background noise and the other-cell MAI become larger. In addition to distance-dependent path loss, shadowing exists. The instantaneous SIR on each forward link channel varies in a random manner. This suggests that the use of fast TPC can increase the link capacity of the forward link as well as that of the reverse link.

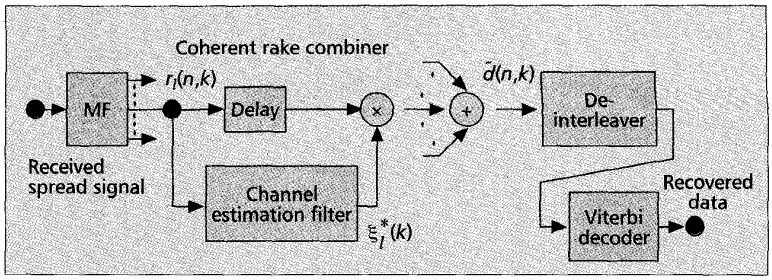

■ **Figure 6.** *Coherent Rake receiver structure.*

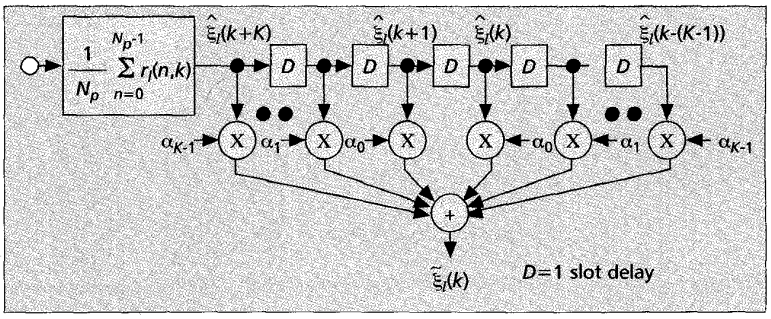

■ **Figure 7.** *WMSA channel estimation filter.*

COHERENT RAKE COMBINING

The coherent Rake receiver structure is illustrated in Fig. 6. The MF resolves the frequency-selective multipath channel into $L(\geq 1)$ frequency-nonselective propagation paths with different time delays (time resolution equals one chip duration T_c). The coherent Rake combiner output is represented at the nth symbol position of the kth slot associated with the lth propagation path, $l = 0, 1, \ldots, L - 1$, as

$$\tilde{d}(n,k) = \sum_{l=0}^{L-1} r_l(n,k)\tilde{\xi}_l^*(k),$$

where $\tilde{\xi}_l(k)$ is the channel estimate. The sequence of $\tilde{d}(n, k)$ is deinterleaved and soft-decision Viterbi decoded to recover the transmitted binary data. Since fading statistics on the reverse link are altered by fast TPC, the Kalman filter theory cannot be applied to derive the optimum channel estimation filter. A pragmatic approach is thus required. A $2K$-tap weighted multislot averaging (WMSA) channel estimation filter is shown in Fig. 7 [6]. Instantaneous channel estimation using the pilot symbols belonging to each slot is performed first, and channel estimates, $\hat{\xi}_l(k + i)$s, of $2K$ succeeding slots

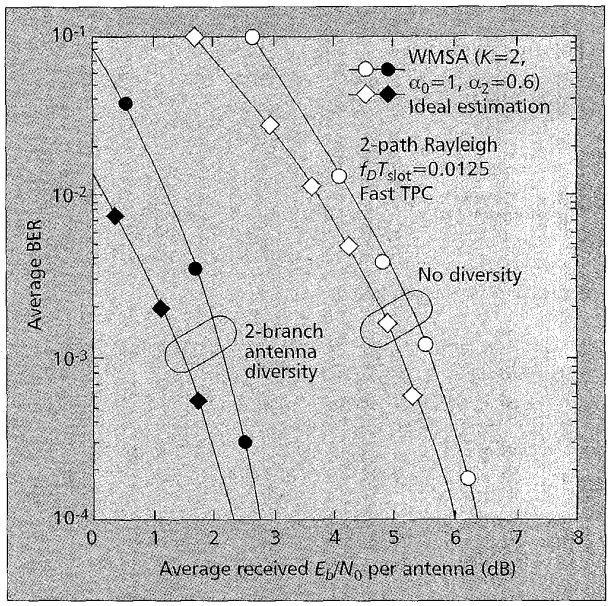

■ **Figure 8.** *BER performance with WMSA coherent Rake receiver.*

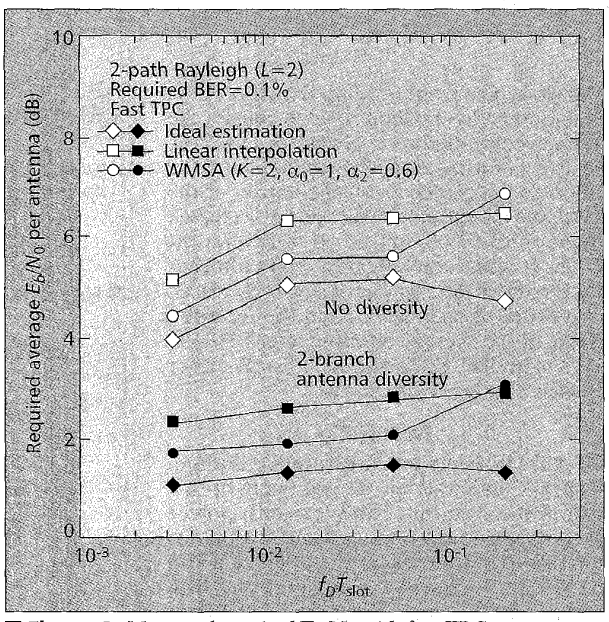

■ **Figure 9.** *Measured required* E_b/N_0 *with fast TPC.*

$(k = -K + 1,..., 0, 1,..., K)$ are then weighted and summed to obtain the final channel estimate $\tilde{\xi}_l(k)$ as

$$\tilde{\xi}_l(k) = \sum_{i=0}^{K-1} \alpha_i \hat{\xi}_l(k-i) + \sum_{i=1}^{K} \alpha_{i-1} \hat{\xi}_l(k+i), \qquad (2)$$

where α_i is the real-valued weight. By selecting the appropriate weights, accurate channel estimation is possible, particularly in slow fading environments, because a large number of pilot symbols belonging to multiple slots can be used. For very slow fading, the $2K$-tap WMSA channel estimation filter increases the signal-to-noise ratio (SNR) of the channel estimate by a factor of

$$N_p \left(\sum_{i=0}^{K-1} \alpha_i \right)^2 \Big/ \sum_{i=0}^{K-1} \alpha_i^2 .$$

As fading becomes faster, however, tracking ability against fading tends to be lost. This is even true for the case of power-controlled links. Although the received signal amplitude is held almost constant by fast TPC, its phase still varies due to fading. However, this is not a problem because channel coding/interleaving works satisfactorily in fast fading. Channel coding/interleaving and fast TPC complement each other in working against fading.

Figure 8 plots the computer-simulated BER performance of the reverse link with fast TPC and WMSA channel estimation filter with $K = 2$ for $f_D T_{slot} = 0.0125$, where $T_{slot} = 0.625$ ms is the slot length (for 2 GHz carrier frequency, $f_D T_{slot} = 0.0125$ corresponds to a traveling speed of 10.8 km/hr). The plotted data was obtained by measuring the average BER and average received E_b/N_0 for various TPC target values. The channel coding assumed was rate-1/3, constraint length of 7-bit convolutional coding. The chip rate of 4.096 Mchips/s and the symbol rate of 64k symbols/s were assumed. $N_p = 4$ pilot symbols were multiplexed in each slot of N_{slot}=40 symbols (10 percent power was allocated to the pilot channel). The performance with WSMA channel estimation ($K = 2$) is close to that of ideal channel estimation. The required E_b/N_0 per antenna for the average BER = 10^{-3} is plotted as a function of $f_D T_{slot}$ in Fig. 9. As expected, with two-branch antenna diversity reception the required E_b/N_0 is relatively insensitive to values of $f_D T_{slot}$.

Instead of using a time-multiplexed pilot, the pilot symbols can be transmitted in parallel with the data channel. The parallel pilot channel is spread by a spreading sequence orthogonal to the data channel. To reduce the amplitude variation of the composite signal, I/Q multiplexing is applied (data and pilot channels are multiplexed onto the in-phase (I) and quadrature phase (Q) of the carrier). If the pilot-to-data power ratio is the same, although the time-multiplexing is slightly superior in fast fading, both multiplexing schemes provide almost the same BER performance over a wide range of f_D values.

Orthogonal Multi-SF Forward Link

As the frequency selectivity of the propagation channel strengthens (or the number of resolvable paths increases), the orthogonality among different users tends to diminish because of increasing inter-path interference; however, orthogonal spreading always gives a larger link capacity than random spreading. This suggests the advantage of using the orthogonal multi-SF codes in the forward link. Multi-SF codes $C_{2m}^{(j)}$, where M is a positive integer and $J = 1, 2,..., 2^m$ can be generated recursively, as shown in Fig. 2, based on a modified Hadamard transformation, resulting in a tree-structured code family [7]. For more detailed description of code generation, refer to [7] or the companion paper [16] of this issue.

Simplified transmitter and receiver structures of the orthogonal forward link data channel are shown in Fig. 10. Data with the symbol rate that equals the chip rate/2^m is spread using a single code with the SF of 2^m, where m is a positive integer. Since a single spreading code can be used at any data rate, the mobile receiver can be significantly simplified compared to the orthogonal multicode forward link which simultaneously uses 2^n codes in parallel, each with an SF of 2^{m+n} where $n \leq m$. Noticing that a lower-layer code can be expressed as an alternate combination of the sequence of its mother code (see Fig. 8 of Ref. [16]), further simplification of code usage is possible. Multi-SF codes of the bottom layer, e.g., codes of 256 chips/symbol, can always be used irrespective of the data rate, and only the integration time at the receiver needs to be changed; the spreading code does not need to be changed to match the data rate.

VARIABLE-RATE TRANSMISSION WITH BLIND RATE DETECTION

In multimedia-type services, the data rate changes time to time or frame by frame during communications. Since all users transmit their signals at the same carrier frequency, each user's received signal suffers from the MAI produced by other users in other cells as well as those in its own cell. Fast and accurate TPC can suppress the MAI. Moreover, variable-rate transmission can also reduce the amount of MAI, thus directly increasing the capacity. Perhaps the simplest variable-rate transmission is to use discontinuous transmission; each slot is partially filled when the data rate is below the maximum while keeping the instantaneous symbol rate the same. By doing so, in the case of the forward link, changing the multi-SF code (or the receiver integration time) according to variations in the data rate is not necessary. If the receiver knows what rates are possible, the transmitted variable-rate data can be recovered without transmitting the rate information (RI); this is called blind rate detection. Blind rate detection is incorporated into the process of Viterbi-decoding the received convolutional-coded frame data. At each possible end bit position in the transmission frame, the surviving path arriving at the zero state in the trellis is selected if its path metric satisfies the following condition [8]:

$$\delta(n_{\text{end}}) = -10\log\left(\frac{\lambda_0(n_{\text{end}}) - \lambda_{\min}(n_{\text{end}})}{\lambda_{\max}(n_{\text{end}}) - \lambda_{\min}(n_{\text{end}})}\right) < \Delta_r \text{ dB}, \quad (3)$$

where $\Delta_r (> 0)$ is the threshold value in dB, $\lambda_{\max}(n_{\text{end}})$ and $\lambda_{\min}(n_{\text{end}})$ are the maximum and minimum path metric values among all survivors at the end bit position, respectively, and $\lambda_0(n_{\text{end}})$ is that at the zero state. If the condition of Eq. 3 is met, the surviving path is traced back to recover the frame data. Cyclic redundancy check (CRC) decoding is then performed to determine whether the recovered data is correct or not. Lowering the value of Δ_r reduces the probability of false rate detection. However, excessively low Δ_r increases the probability of frame error because the probability of the correct trellis path being selected decreases. Figure 11 compares the frame error rate (FER) performance of variable-rate transmission with blind rate detection using $\Delta_r = 2$ and ∞ dB with that of 3-bit RI-assisted rate detection. Blind rate detection with $\Delta_r = 2$ dB provides almost the same FER performance as RI-assisted rate detection with the same overhead, and the performance is very close to the lower bound (known rate case).

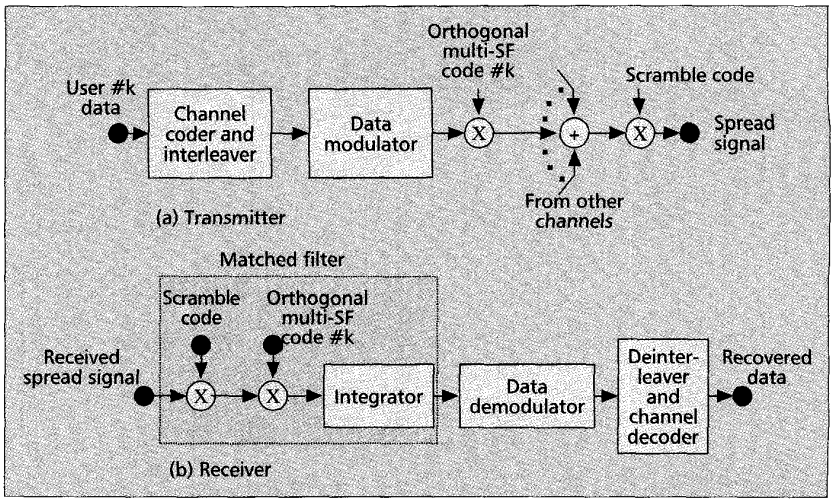

■ **Figure 10.** *Orthogonal forward link transmitter and receiver structure.*

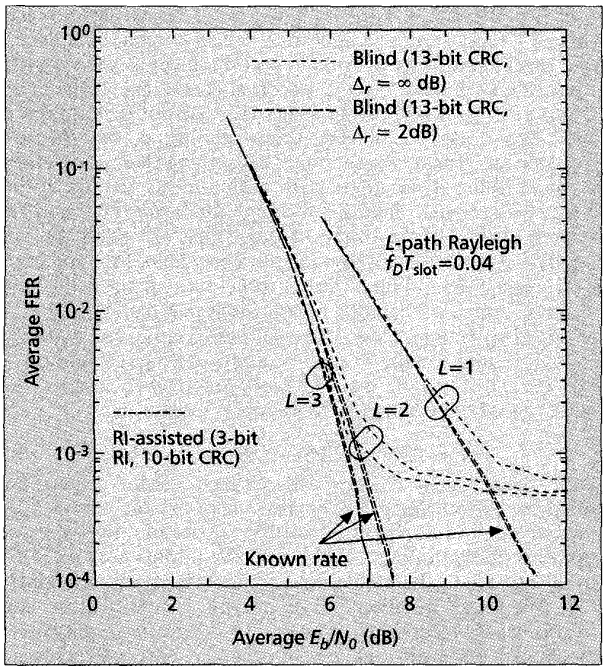

■ **Figure 11.** *Variable rate transmission performance with blind rate detection.*

Another variable-rate transmission scheme with blind rate detection is to vary both the transmit power and the spreading factor according to the data rate, while keeping the chip rate the same (resulting in continuous transmission). The data symbol sequence is multiplied by one of the orthogonal codes chosen from the code family of the previous subsection according to the data rate before applying spreading modulation to make all symbol sequences with different rates orthogonal. At the receiver, noncoherent orthogonal demodulation is applied for rate detection. One orthogonal code set is (01, $0^2 1^2$, $0^4 1^4$, $0^8 1^8$, ...). Code 01 is multiplied onto the maximum rate data, and code $0^k 1^k$ is multiplied onto the data with 2^k times lower rate than the maximum. As the rate observation time progresses (from the beginning of the frame), the rate detection probability continuously improves. Since the blind rate detection process of this variable-rate transmission scheme is separate from the channel decoding process of the data channel, data channels of different rates can be multiplexed and demultiplexed without RI. Noncoherent orthogonal demodulation can be repeatedly performed on a despread signal sequence sampled and stored at the sampling rate of twice the maximum data rate.

FIELD EXPERIMENTS

An experimental W-CDMA system was constructed whose radio link parameters were slightly different from those introduced in the previous section; chip rates of 1.92, 3.84, 7.68, and 15.36 Mchips/s were used, and the slot length was T_{slot} = 1.25 ms (8 slots/frame). The carrier frequencies of the forward and reverse links were 2.175 GHz and 1.9905 GHz, respective-

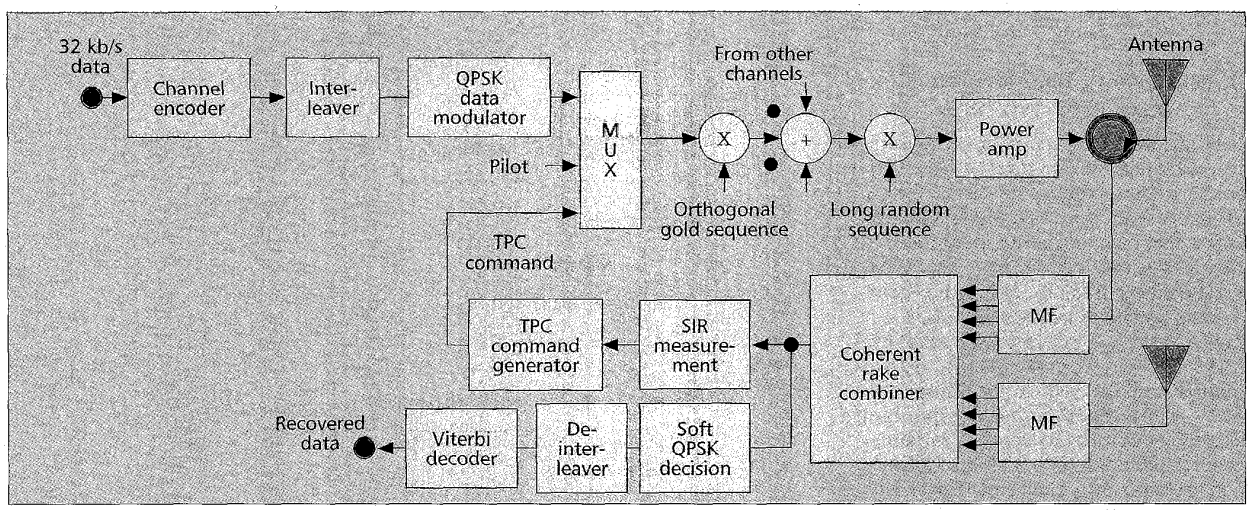

■ **Figure 12.** *Simplified block diagram of base station transceiver.*

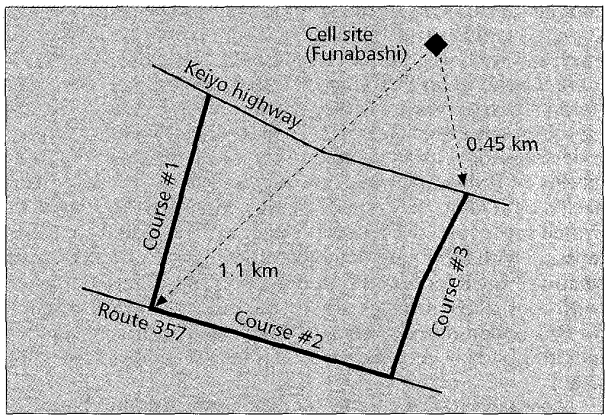

■ **Figure 13.** *Measurement courses.*

ly. Field experiments were conducted in Tokyo [9]. We focused on the reverse link performance of 32 kb/s transmission. Measured results for the average BER performance and the effect of spreading bandwidth on the mobile transmit power are presented. Also presented is the measurement result of 1.92 Mb/s data transmission [10].

System Set-up for 32kb/s Data Transmission

The base station transceiver is illustrated in Fig. 12. The channel encoder was a rate-1/3, constraint length k = 7-bit convolutional encoder. The interleaved coded data sequence of one frame was transformed into a QPSK-modulated symbol sequence and multiplexed every 1.25 ms with N_p = 4 pilot symbols and the TPC command (1 symbol). The QPSK symbol rate was 60 ksymbols/s. The spreading factor was thus, 128chips/symbol for 7.68 Mchips/s spreading. In the experimental system, up to 24 channels were available. In the forward link, orthogonally spread signals were summed and then, binary phase shift keying (BPSK)-modulated by a single scramble code (2^{33} – 1 chip sequence). On the other hand, for the reverse link the QPSK symbol sequence was directly BPSK-spread using a long random sequence (2^{33} – 1 chip sequence). Finally, the spread signal was power-amplified and transmitted.

The power delay profile was measured over an interval of 50ms using the MF output to select the four strongest paths per antenna for coherent Rake combining. A first order interpolation filter was used instead of the WMSA channel estimation filter. A first order interpolation filter was used instead of the WMSA channel estimation filter. The Rake combiner output sample sequence was then transformed into a soft-decision sample sequence, followed by the operation of deinterleaving and soft-decision Viterbi decoding to recover the transmitted data. The TPC command was transmitted every 1.25 ms to the mobile via the forward link to raise or lower the transmit power by 1 dB (TPC delay was three-slot).

Measurement Course Characterization

The field experiment area is illustrated in Fig. 13. The heights of the cell site and mobile station antennas were 59 m and 2.9 m from the ground, respectively. The maximum allowable transmit power of the mobile station was 2 W. A measurement vehicle equipped with the mobile station was driven along measurement courses #1–#3, at distances of 0.45–1.1 km from the center cell site, at speeds of 10–40 km/hr. The right side of course #1 is a factory area, the left side a mixture of a school campus, factories, tall apartment complexes, and individual houses. An elevated highway is seen on the right side of course #2, and its left side is a residential area. Course #3 passes through a factory area and a residential area. When using 7.68 Mchips/s spreading, course #1 first experiences clear two-path fading having almost equal average powers, followed by single-path fading in the middle of the course. Three-path fading having unequal average powers is seen at the end of the course. Along course #2, two-path fading having almost equal average power appears first, followed by a single path and then two- to three-path fading at the end. Most of course #3 exhibits two-to-three path fading. For 3.84 Mchips/s spreading, most of the courses experienced two-path fading, except for the middle sections of courses #1 and 2; however, only single-path fading appeared in most of the courses for both 0.96 and 1.92 Mchips/s spreading.

The Effect of Spreading Bandwidth

Here, the effects of the spreading chip rate on the reverse link transmit power and BER performance are discussed. The measured cumulative distribution of the mobile transmit power is plotted in Fig. 14. The transmit powers are expressed in dB relative to the median (50 percent) transmit power with 0.96 Mchips/s spreading and no antenna diversity at the cell site. Diversity reception can reduce the mobile transmit power by about 3 dB at the median value. As the chip rate increases, the probability of large transmit powers reduces because the multipath time resolution capabilities improve and the fading

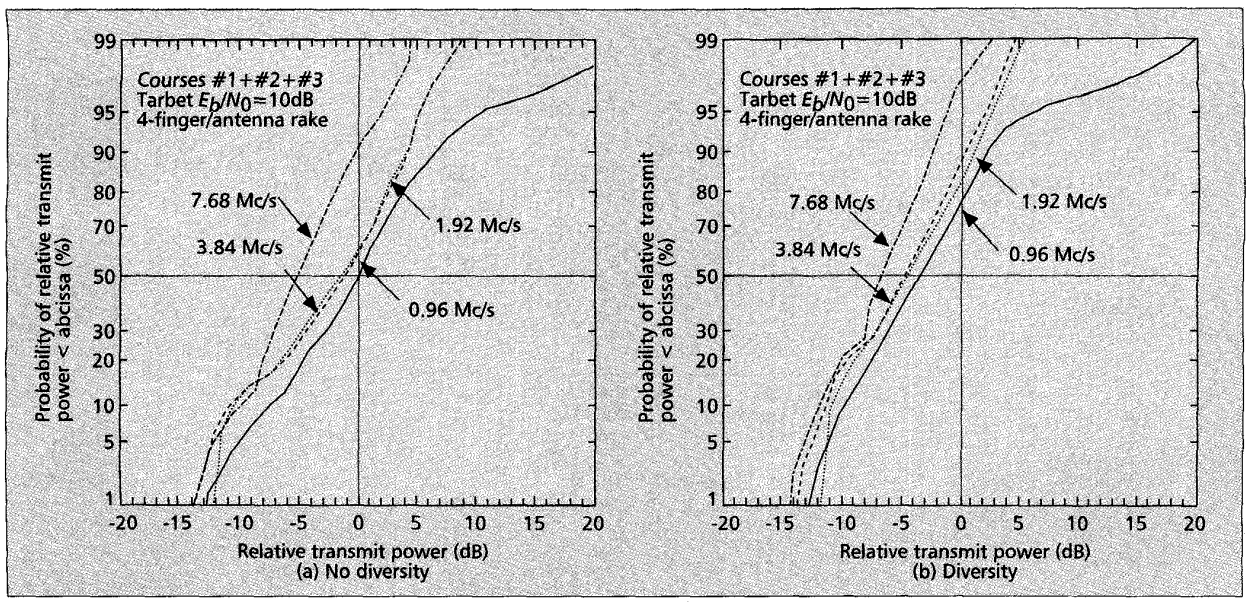

■ **Figure 14.** *Comparison of mobile transmit powers with different chip rates.*

seen after Rake combining becomes shallower. Fast TPC compensates for the fading seen after Rake combining. As a consequence, the probability of large transmit powers falls as chip rate increases. When the chip rate increases from 0.96 to 3.84 Mchips/s, the reduction in the median transmit power is 1.2 dB. The use of 7.68 Mchips/s further reduces the median transmit power by about 4 dB. A similar power reduction as the chip rate increases can also be seen when antenna diversity is applied.

The measured BER performance is plotted as a function of target E_b/I_0 at the Rake combiner output in Fig. 15 with the spreading chip rate as a parameter. For comparison, the computer simulation results are also plotted for different numbers L of resolved paths. Without antenna diversity, as the chip rate increases the BER performance improves; while the BER performance with 0.96 Mchips/s spreading is close to the computer-simulated BER performance with L = 1, the performance with 7.68 Mchips/s spreading becomes almost

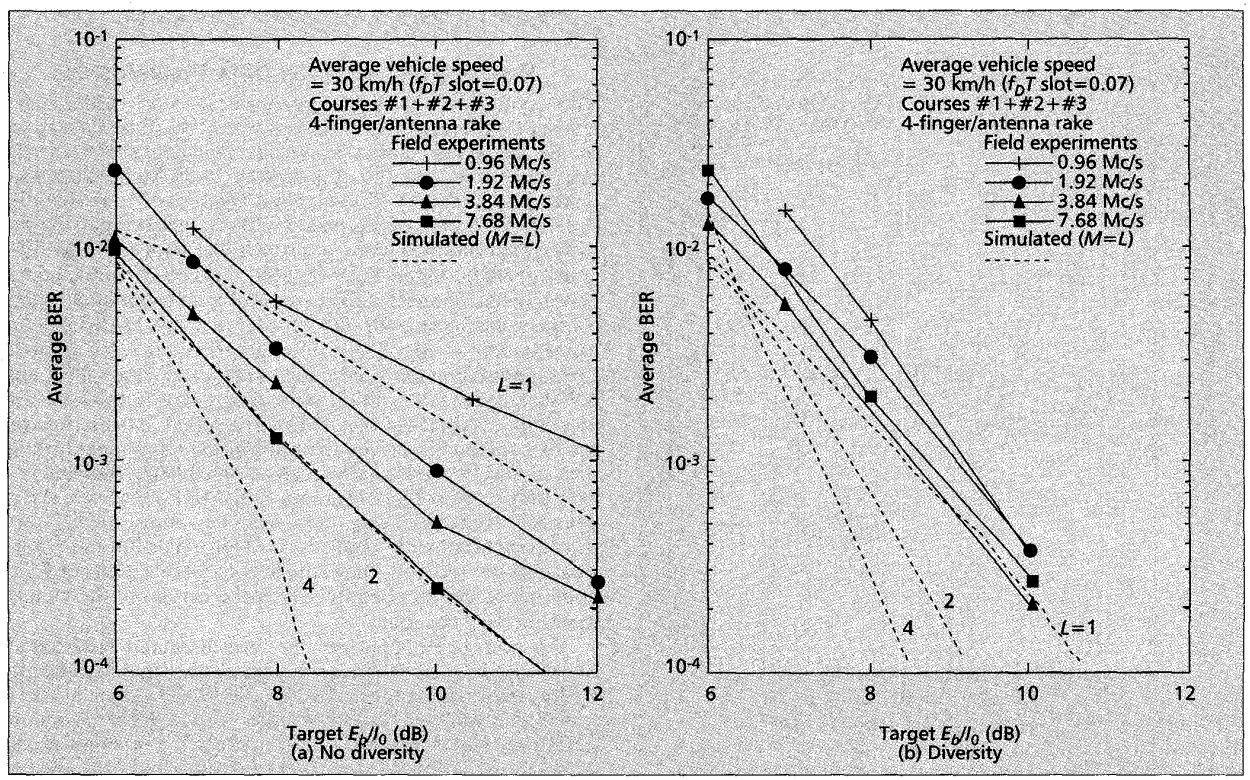

■ **Figure 15.** *Comparison of average BER performance with different chip rates.*

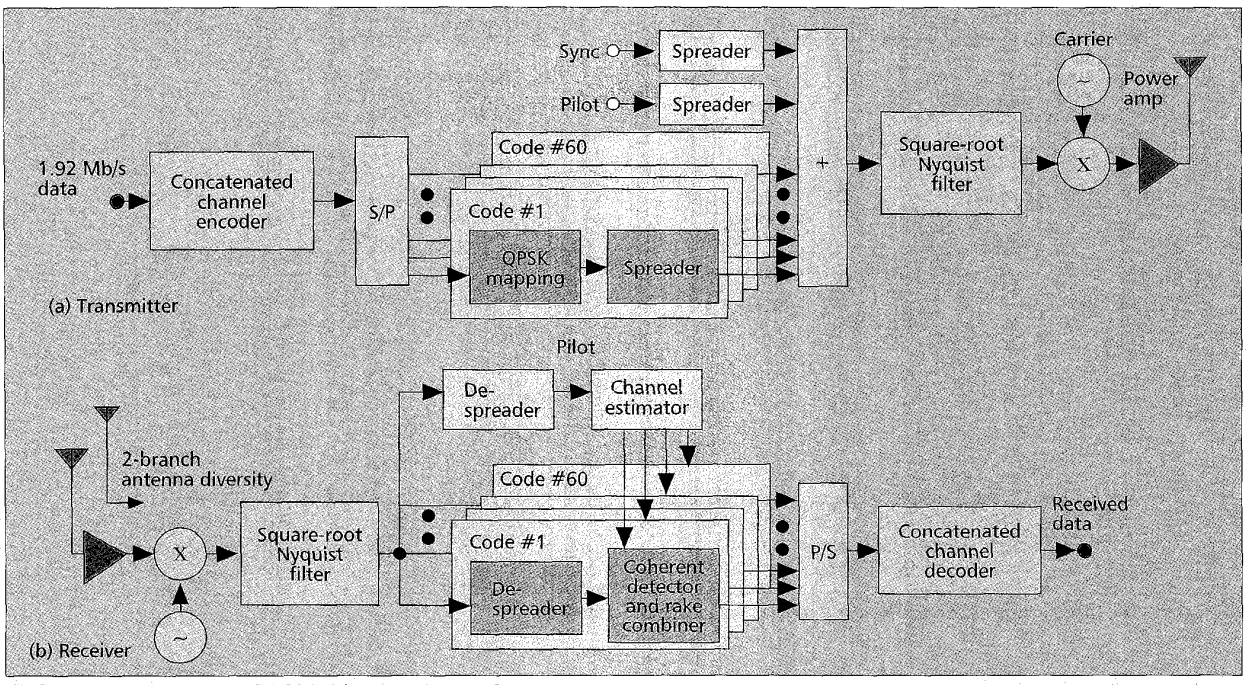

■ **Figure 16.** *Experimental 1.92 Mb/s transmitter and receiver.*

the same as the simulated performance with $L = 2$. When antenna diversity is used, the BER performance improvements achieved by increasing the chip rate are not significant compared to those without diversity, as can be expected from the computer simulation. However, it should be pointed out that increasing the chip rate from 0.96 to 7.68Mchips/s can reduce the median transmit power by about 4 dB with antenna diversity. The results may depend on the surrounding environment, so further measurements in different places are required. It also be noted that if the $K = 2$ WMSA channel estimation filter is used instead of the first order interpolation filter, the TPC rate increased from 800Hz to 1600Hz, and furthermore the TPC delay is reduced to one slot, the achievable BER performance of Fig. 15 can be improved by about 2–3 dB.

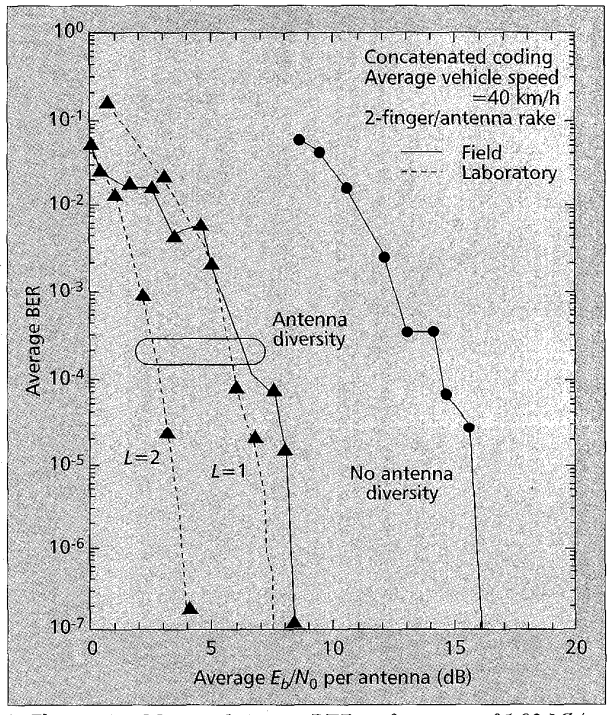

■ **Figure 17.** *Measured average BER performance of 1.92 Mb/s data.*

High-Speed (1.92 Mb/s) Data Transmission

The structure of an experimental 1.92 Mb/s data transmitter/receiver is illustrated in Fig. 16. It was based on the 62-channel orthogonal multicode approach, each transmitting 32 kb/s data at the chip rate of 15.36 Mchips/s (radio bandwidth 20 MHz). Two channels were used to realize the parallel pilot and synchronization. Note that by applying the orthogonal multi-SF code approach, the number of parallel codes could be significantly reduced. Instead of turbo coding, concatenated channel coding — rate-1/3 convolutional coding for inner coding and RS (40, 32) coding with 8 bits/symbol for outer coding — and 80 ms outer interleaving were applied. Data modulation and spreading modulation were QPSK and BPSK, respectively, and the spreading factor in this case was 256 chips/symbol. No fast TPC was applied. At the receiver the two antennas received the transmitted 62-channel orthogonal multicode signal, each received signal being sampled at a rate of 4 x 15.36 MHz using an 8-bit A/D converter. After channel estimation using $N_p = 4$ pilot symbols, the MF outputs associated with each resolved propagation path were phase-corrected and time-adjusted to allow coherent Rake combining. The total number of Rake fingers of the experiment receiver was four.

The average BER performance was measured while traveling at speeds of 10–40 km/hr to demonstrate that high-quality 2 Mb/s transmission over a real 2 GHz W-CDMA radio link is possible in vehicular environments. Although the measured BER sometimes approached 0.01 when the received E_b/N_0 dropped, BERs better than 10^{-6} were achieved over most of the measurement course. The measured average BER perfor-

mance is plotted in Fig. 17. The BER performance with diversity reception under a real fading environment is degraded compared to those of a laboratory experiment with simulated fading environments with $L = 1$ and 2. However, as expected from the laboratory measurements, antenna diversity reception can significantly improve transmission performance, and BERs of better than 10^{-6} can be achieved for average $E_b/N_0 > 9$ dB while the mobile station is driven at a speed of 40 km/hr.

Enhanced Radio Transmission Techniques

For the isolated cell case, the link capacity of DS-CDMA is much smaller than TDMA and frequency-division multiple access (FDMA) because the DS-CDMA link is interference-limited. However, in the DS-CDMA cellular systems, the introduction of sectored cells and also the reuse of the same carrier frequency at all cells overcome this disadvantage. Reducing the MAI can further increase the link capacity. One candidate is the interference canceller and another is the adaptive antenna array which can be viewed as adaptive sectorization.

Multi-Stage Interference Canceller

Interference cancellers (ICs) can be basically classified into the single-user type and the multi-user type. The former reduces the MAI using a linear filter (one example), and is simpler to implement than the latter. W-CDMA uses long random spreading code sequences on the forward link for scrambling and on the reverse link and thus, the time-varying nature of spreading code sequence, when observed over every one symbol period, excludes adoption of the single user type. One multi-user IC receiver is the decorrelating receiver. This requires very complex computation of the inverse correlation matrices among different users' spreading codes and is considered impractical. On the other hand, the multi-stage IC version of the non-linear replica generation type [11] is attractive since interference replica generation and subtraction is done successively for different users. Accurate channel estimation is required to generate the interference replica of each user. This can be accomplished by exploiting the pilot symbols. The resulting multi-stage IC is called the coherent multi-stage IC (COMSIC hereafter) [12]. The channel estimate is updated at succeeding stages for each user, which results in improved channel estimation compared to the one-time channel estimation in the first stage and leads to increased link capacity.

Figure 18 illustrates the simplified structure of the COMSIC receiver. The received signal power of each user is measured after matched filtering and users are ranked in order of decreasing power. The ranking is updated every slot. Each stage has K channel estimation-and-interference replica generation units (CEIGUs), where K is the number of simultaneously communicating users, and each performs matched filtering (de-spreading), channel estimation, tentative symbol decision, and replica generation of each user in order of decreasing power. Without loss of generality, the received signal powers are assumed to decrease as the user index $\#k$ increases and the resolved propagation paths are also indexed in order of decreasing power. Before each CEIGU, the interference replicas of K-1 users are subtracted from the received

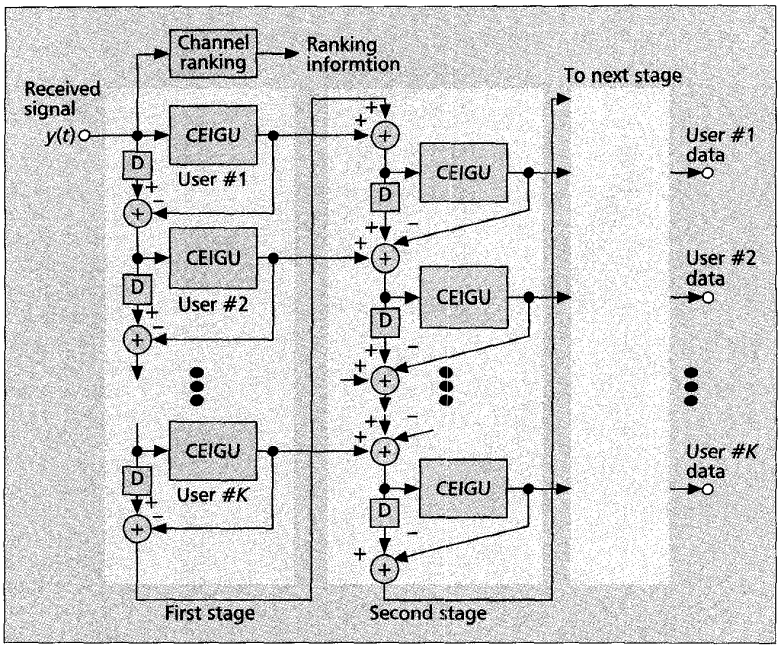

■ **Figure 18.** *COMSIC receiver structure.*

spread signal $y(t)$. Letting $\hat{I}_{i,l}^{(p)}(t)$ be the generated interference replica, at the p-th stage, of the i-th user associated with the l-th path, the input $y_k^{(p)}$ to the p-th stage, k-th user CEIGU can be represented as

$$y_k^{(p)}(t) = \begin{cases} y(t) - \sum_{i=1}^{k-1}\sum_{l=0}^{L-1} \hat{I}_{i,l}^{(1)}(t-\hat{\tau}_{i,l}) & \text{for } p=1 \\ y(t) - \left[\sum_{l=0}^{L-1}\sum_{\substack{j=0 \\ j\neq l}}^{l-1} \hat{I}_{k,j}^{(p-1)}(t-\hat{\tau}_{k,j} + \sum_{i=1}^{k-1}\sum_{l=0}^{L-1} \hat{I}_{i,l}^{(p)}(t-\hat{\tau}_{i,l}) \right. & \\ \qquad \left. + \sum_{i=k+1}^{K}\sum_{l=0}^{L-1} \hat{I}_{i,l}^{(p-1)}(t-\hat{\tau}_{i,l}) \right] & \text{for } p \geq 2 \end{cases} \quad (4)$$

where the first term in the square brackets for $p \geq 2$ is the interpath interference of its own signal, L is the number of resolved paths (here, we assume the same L for all users), and $\hat{\tau}_{i,l}$ is the estimated time delay of the l-th path. Matched filtering on $y_k^{(p)}(t)$ provides the resolved signals

$$\left\{ r_{k,l}^{(p)} \right\}_{l=0}^{L-1}$$

on which channel estimation using pilot symbols is performed for coherent Rake-combining. After tentative symbol decision, $\hat{I}_{k,l}^{(p)}(t)$ is generated as $\hat{I}_{k,l}^{(p)}(t) = \hat{\xi}_{k,l}^{(p)}(t)\,\hat{d}_k^{(p)}(t)c_k(t)$, where $\hat{\xi}_{k,l}^{(p)}(t)$, $\hat{d}_k^{(p)}(t)$, and $c_k(t)$ are channel estimate, tentatively detected symbol, and spreading code sequence, respectively (the continuous time representation is used for simplicity). Since the interference subtraction and channel estimation operation is performed for each user in order of decreasing received power, accuracy of channel estimation can improve for lower ranked users. Furthermore, since channel estimation is repeated for the same user at succeeding stages, the accuracy of channel estimation improves with stage number. The coherent Rake combiner output

$$\tilde{d}_k(t) = \sum_{l=0}^{L-1} r_{k,l}^{(P)}(t)\hat{\xi}_{k,l}^{(P)*}(t)$$

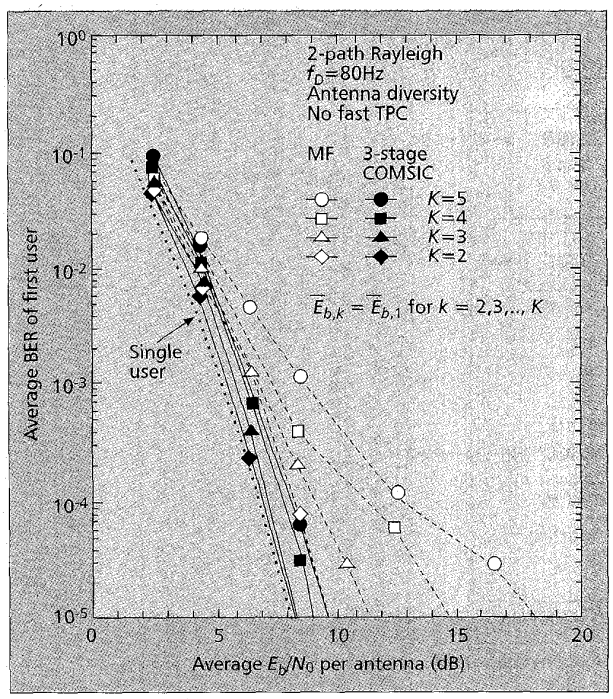

■ **Figure 19.** *Measured average BER performance with three-stage COMSIC*

at the final stage P is the soft decision sample for succeeding deinterleaving and Viterbi decoding.

An experimental COMSIC receiver with $P = 3$ and $L = 8$ was implemented for the chip rate of 1.024 Mchip/s and the spreading factor of 16 chips/symbol. Channel coder and data frame structure were the same as presented previously. The average BER performance obtained from laboratory experiments using a hardware-fading simulator is plotted in Fig. 19 as a function of average E_b/N_0 for various numbers K of active users. The power delay profile was a two-path profile, each path being subjected to independent Rayleigh fading with equal average power and f_D = 80 Hz. The average BER with 3-stage COMSIC monotonically falls as the average E_b/N_0 increases, while that with MF receiver approaches an error floor that depends on the number, K, of users. However, as K increases, the E_b/N_0 loss from the single-user case increases due to the residual MAI. When K = 8, however, the E_b/N_0 loss at the BER of 10^{-3} is only about 2.5–3 dB.

The regenerated interference replica is perturbed by the channel estimation error. Weighting (by a factor of less than one) the regenerated interference replicas before subtraction from the received signal can further improve BER performance.

An Adaptive Antenna Array Combined with a Rake Receiver

The adaptive antenna array directs beam nulls to interference sources to maximize the SIR of each user [13]. In W-CDMA mobile radio, the adaptive antenna array can be combined with the coherent Rake receiver [14]. This is called the coherent adaptive antenna array Rake receiver (CAAAR receiver hereafter). In the case of voice-only services, the application of the CAAAR receiver is rather impractical because a large number of antenna elements is required. The CAAAR receiver is particularly useful for multimedia communications in which different users are transmitting with different data rates. High-rate users, although their number is not large, cause significant interference to low-rate users (particularly voice users); thus, without an adaptive antenna array, the link capacity in terms of users/cell/MHz would be reduced significantly.

It is interesting to compare the adaptive antenna array with the fixed multibeam antenna. For the latter, the cell site receiver associated with a particular user selects the optimum beam from the fixed multiple beams formed by a beamformer. Although a fixed multibeam antenna seems much simpler to implement, the CAAAR receiver in a W-CDMA system has the following three advantages. First, the multibeam antenna receiver cannot change the beam direction finely while the CAAAR receiver can. Second, at the beginning of communication, the multibeam antenna receiver must find the arrival angle of the desired user by switching the beams, while the CAAAR receiver starts from the omnibeam pattern and forms the optimum beam pattern quickly by the aid of an adaptation algorithm. The arrival angles of incoming radio signals, each having propagated along a resolved path, are not necessarily the same; they may be widely spread, particularly in a microcellular system. Thus, third, the CAAAR receiver can be designed to direct the beam toward each resolved path of each user and to realize coherent Rake combination even though their angles are quite different.

An important issue with the CAAAR receiver, when applied to mobile communications, is how accurately the antenna beam pattern should be adapted for each moving user. Both the known pilot symbols, received periodically, and data symbols can be exploited for this purpose. The block diagram of a decision-directed coherent CAAAR receiver is illustrated in Fig. 20. Let the number of antenna elements be J. The antenna beam pattern for the lth resolved path of the kth user is formed to maximize the average SIR of the combined signal sequence given by

$$z_{k,l}(m) = \sum_{j=1}^{J} r_{k,l}^{(j)}(m) w_{k,l}^{(j)*}(m),$$

$m = \ldots, -1, 0, 1, 2, \ldots$ (symbol position), where $r_{k,l}^{(j)}(m)$ and $w_{k,l}^{(j)*}(m)$ are the resolved modulated signal sample received

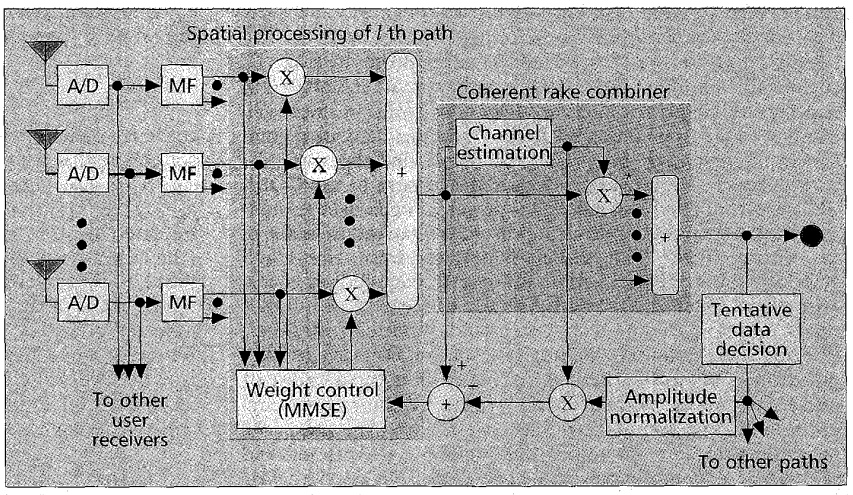

■ **Figure 20.** *Block diagram of CAAAR receiver.*

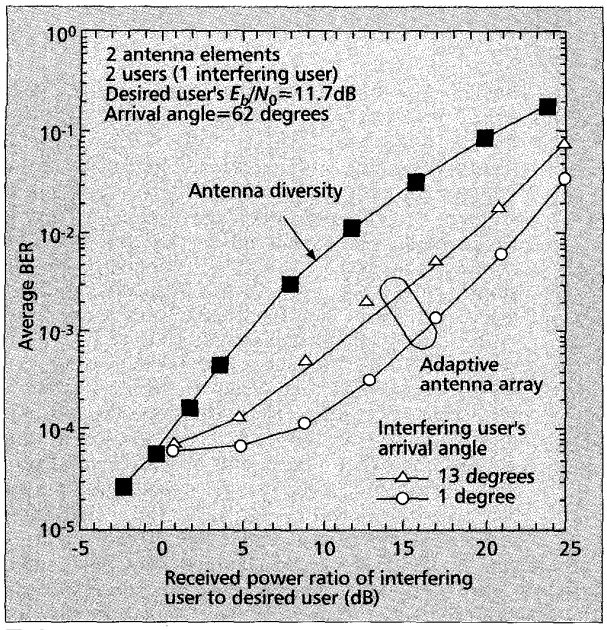

■ **Figure 21.** *Measured average BER as a function of received power ratio of interfering user to desired user.*

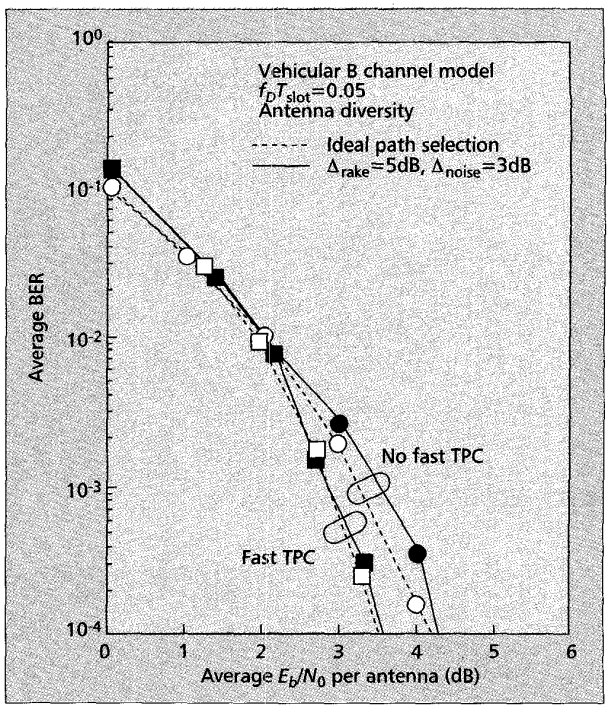

■ **Figure 22.** *Average BER performances with MF-based Rake receiver.*

on the jth antenna element and the associated antenna weight, respectively. Channel estimation is performed on $z_{k,l}(m)$ using received pilot symbols, and then signal samples $\{z_{k,l}(m)\}_{l=0}^{L-1}$ are coherent Rake-combined as described previously. The weights $[w_{k,l}^{(j)}*(m)\}_{j=1}^{J}$ are updated based on the normalized least mean square (LMS) adaptation algorithm so that the mean square error of $z_{k,l}(m)$ with respect to a reference $\hat{z}_{k,l}(m)$ is minimized:

$$w_{k,l}^{(j)}(m+1) = w_{k,l}^{(j)}(m) + \mu \frac{r_{k,l}^{(j)}(m-(N_p+N_d))}{\sum_{j=1}^{J}\left|r_{k,l}^{(j)}(m-(N_p+N_d))\right|^2} e_{k,l}^{*}(m-(N_p+N_d)), \quad (5)$$

where $e_{k,l}(m)$ is the instantaneous error defined as $e_{k,l}(m) = \hat{z}_{k,l}(m) - z_{k,l}(m)$ and μ is the step size. Both pilot symbols and tentatively recovered data symbols can be used as a reference. Since channel estimation using time-multiplexed pilot symbols incurs one time slot delay, the instantaneous error at the mth time position of the previous slot is used for weight updating; the slot length in symbols is N_p (pilot) + N_d (data including TPC command).

A preliminary laboratory experiment assuming two users (one desired user and one interfering user) was conducted using a two-path Rayleigh fading hardware simulator. For a performance comparison of CAAAR and two-antenna diversity reception, the measured average BERs of a simple two-element CAAAR receiver are plotted in Fig. 21 as a function of received power ratio of interfering user to desired user. The data rate and the chip rate are 64 kymbols/s and 4.096Mchips/s, respectively. μ was assumed to be 10^{-4}. In this experiment, the two simulated paths arrive from the same direction. The average E_b/N_0 and the arrival angle of the desired user were set to 11.7 dB and 62°, respectively. The average BER can be reduced by about one order of magnitude compared to the antenna diversity case even if the interfering user's power is 10 dB higher (this corresponds to the situation of 10 interfering users or a single user with 10 times higher data rate). The improvement offered by the adaptive antenna array diminishes as the arrival angle of the interfering user's signal approaches that of the desired user's signal. When two users are within the beamwidth, either one should be blocked. However, the probability of blocking can be made much smaller than that without adaptive antenna array diversity.

Matched Filter Rake Receiver

More rapid spreading code acquisition is possible with the MF compared to the synchronous correlator. Since the MF provides G_s (spreading factor) despread signal components (the time delay resolution is one chip duration) at each symbol timing, an MF-based Rake combiner is much simpler to implement than a synchronous correlator-based Rake combiner. As the spreading bandwidth increases, the number of resolvable paths increases, which makes the MF-based Rake combiner more attractive. Note that the spreading code sequence over the one symbol period must be changed symbol by symbol when a long scramble code is used as previously mentioned.

An important design problem with the Rake combiner is how to select the resolved paths that provide sufficiently large SIR. Two thresholds can be introduced for this purpose: the first selects paths having sufficiently large signal powers within a certain dB range below the maximum, and the second discards noise or noise-only paths among those selected by the first threshold. Path selection is done using the measured power delay profile. The instantaneous power $\hat{S}_l(k)$ of the lth path (l = 0, 1, ..., G_s – 1) of the kth slot is measured and then averaged by a simple first-order filter to obtain the delay power profile

$$\left\{\overline{S}_l(k)\right\}_{l=0}^{G_s-1}: \overline{S}_l(k) = \alpha\overline{S}_l(k-1) + (1-\alpha)\hat{S}_l(k),$$

$$\hat{S}_l(k) = \left|\hat{\xi}_l(k)\right|^2,$$

where $\hat{\xi}_l(k)$ is the instantaneous channel estimate obtained from pilot symbols belonging to the k-th slot and α is the for-

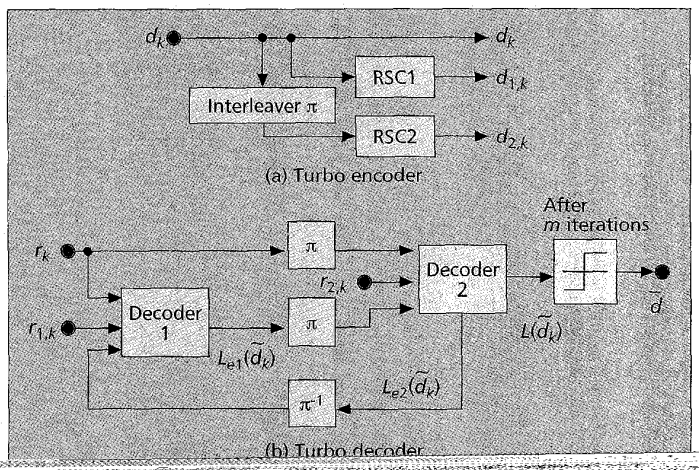

Fig. 23. The encoder consists of two rate-1/2, constraint length $K = 3$ recursive systematic convolutional encoders, RSC1 and RSC2, and a pseudo-random interleaver π. The turbo-coded sequence $[d_k, d_{1,k}, d_{2,k}; k = 0, 1, ..., N - 1]$, where N denotes the length of information sequence $\{d_k\}$ is transmitted after channel interleaving over the radio channel and received as the soft decision sample sequence $\{r_k, r_{1,k}, r_{2,k}\}$. In the iterative decoding algorithm, the first soft-in/soft-out decoder computes the so-called extrinsic information $\{L_{e1}(\tilde{d}_k)\}$, where $\{\tilde{d}_k\}$ is the estimate of $\{d_k\}$. The second soft-in/soft-out decoder then computes the new extrinsic information $\{L_{e2}(\tilde{d}_k)\}$ using the previous extrinsic information for feeding back to the first soft-in/soft-

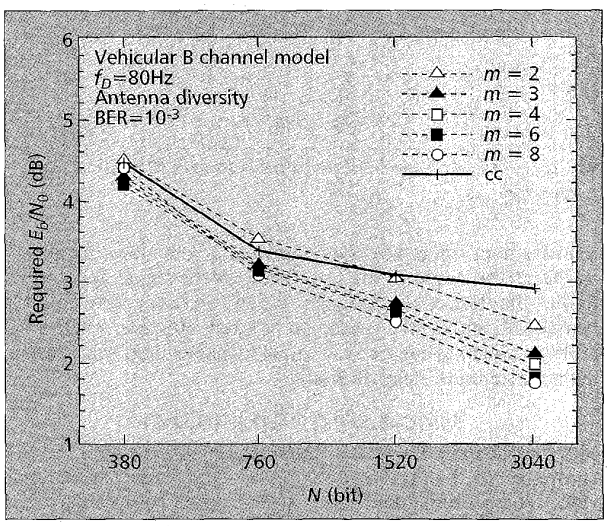

Figure 24. *Turbo coding effect on required* E_b/N_0.

getting factor (the equivalent measurement interval is given by $T_{slot}/(1-\alpha)$). The paths, satisfying the condition $\bar{S}_l(k) \geq \max\{S_{min}(k) \cdot 10^{0.1\Delta_{noise}}, S_{max}(k) \cdot 10^{-0.1\Delta_{rake}}\}$, are selected every slot for coherent Rake combining, where $S_{min}(k) = \min_l \{\bar{S}_l(k)\}$, $S_{max}(k) = \max_l \{\bar{S}_l(k)\}$ with Δ_{rake} and Δ_{noise} are design parameters. Figure 22 plots the average BER performance obtained from the computer simulation for the power delay profile of the ITU-R Vehicular-B model and $f_D T_{slot} = 0.05$. Channel coding/interleaving is the same as described previously. $\Delta_{rake} = 5$ dB and $\Delta_{noise} = 3$ dB were assumed. For comparison, the BER performance when the paths to be combined are ideally selected is also plotted. The E_b/N_0 loss from the ideal path selection case is less than 0.5 dB both with and without fast TPC.

Turbo Codes

Recently, turbo coding [15] has been attracting much attention because of its relatively large coding gain with reasonable computation complexity. The main features of turbo coding distinguishing it from conventional concatenated coding are:

- Concatenating two or more recursive systematic codes
- Using a pseudo-random interleaver
- Iterative decoding algorithm

An example of a rate-1/3 turbo encoder/decoder is shown in

posteriori probability $\{L(\tilde{d}_k)\}$, on which final sequence detection is made. The effect of adding turbo coding to W-CDMA was evaluated by computer simulation. Figure 24 plots the computer simulation results on the required E_b/N_0 for BER = 10^{-3} as a function of N for various values of m. Multipath Rayleigh fading with the ITU-R Vehicular-B model with $f_D = 80$ Hz and a two-finger/antenna coherent Rake receiver were assumed. The information sequence length was the same as the interleaver size. For comparison, the result for rate-1/3 convolutional codes, denoted cc, with polynomial (554, 624, 764) in octal notation and constraint length $K = 7$ is also plotted; its channel interleaver size is the same as that of the channel interleaver after the turbo encoder. While the performance difference between turbo codes and convolutional codes is negligible for small N (< 760 bits), turbo codes provide superior performance for large N (> 1520 bits). As the value of m increases, the performance improves, but the reduction rate of the required E_b/N_0 becomes smaller for $m > 4$. When $m = 8$ is used, about 1 dB coding gain is obtained over convolutional codes in the case of $N = 3040$ bits, so turbo codes are particularly attractive in data services that permit longer transmission delay.

Conclusion

It is strongly anticipated that the wireless access of IMT-2000 systems (third-generation mobile communications systems) will be based on W-CDMA. This article reviews the technical features of W-CDMA. The significant concept distinguishing it from current IS-95-based systems is the introduction of intercell *asynchronous* operation, which is vital for continuous system deployment from outdoors to indoors, and the data-channel-associated pilot channel for coherent detection. The pilot channel associated with individual data channels facilitates the application of interference cancellation and adaptive antenna array on both reverse and forward links to significantly increase the link capacity and coverage. The use of orthogonal multi-SF codes on the forward link offers very high flexibility in supporting a wide range of multirate services as well as basic services (voice and voiceband data) and can also simplify the mobile receiver structure. Field experiments conducted in Tokyo demonstrated that widening the spreading bandwidth can increase the link capacity as well as reducing the mobile transmit power. Furthermore, we succeeded in 1.92 Mb/s data transmission over a real 2 GHz W-CDMA radio link while traveling.

A fixed wireless access system that supports multimedia communications is also important in the 21st century. This can

also be realized using the W-CDMA technology presented in this article. The orthogonal multi-SF code-multiplexing technique can allow flexible multiple multirate connections to each user.

ACKNOWLEDGMENTS

The authors would like to thank H. Andoh, S. Tanaka, K. Okawa, K. Higuchi, S. Fukumoto, S. Abeta, A. Fujiwara, and A. Shibutani of the Wireless Access Laboratory for their contributions to the W-CDMA computer-simulations and experiments.

REFERENCES

[1] Special Issue, IMT-2000: Standards Efforts of the ITU, *IEEE Pers. Commun.*, vol. 4, Aug. 1997.

[2] A. J. Viterbi, *CDMA, Principles of Spread Spectrum Communications*, Addison-Wesley, 1995.

[3] F. Adachi *et al.*, "Coherent multi-code DS-CDMA mobile radio access," *IEICE Trans. Commun.*, vol. E79-B, Sept. 1996, pp. 1316–25.

[4] U.-C. Fiebig *et al.*, "Design study for a CDMA-based third generation mobile radio system," *IEEE JSAC*, vol. SAC-12, May 1994, pp. 733–43.

[5] K. Higuchi, M. Sawahashi, and F. Adachi, "Fast cell search algorithm in DS-CDMA mobile radio using long spreading codes," *IEICE Trans. Commun.*, vol.E81-B, July 1998, pp. 1527–1534.

[6] H. Andoh, M. Sawahashi, and F. Adachi, "Channel estimation using time-multiplexed pilot symbols for coherent Rake combining for DS-CDMA mobile radio," *IEICE Trans. Commun.*, vol. E81-B, July 1998, pp. 1517–1526.

[7] F. Adachi, M. Sawahashi, and K. Okawa, "Tree-structured generation of orthogonal spreading codes with different lengths for forward link of DS-CDMA mobile radio," *Elect. Lett.*, vol. 33, Jan. 1997, pp. 27–28.

[8] Y. Okumura and F. Adachi, "Variable-rate data transmission with blind rate detection for coherent DS-CDMA mobile radio," *IEICE Trans. Commun.*, vol.E81-B, July 1998, pp. 1365–1373.

[9] T. Dohi, Y. Okumura, and F. Adachi, "Further results on field experiments of coherent wideband DS-CDMA mobile radio," *IEICE Trans. Commun.*, vol. E81-B, June 1998, pp. 1239–47.

[10] K. Okawa, M. Sawahashi, and F. Adachi, "1.92 Mb/s data transmission experiments over a coherent W-CDMA radio link," *IEICE Trans. Commun.*, vol.E81-B, July 1998, pp.1330–1336.

[11] Y. C. Yoon *et al.*, "A spread-spectrum multiaccess system with cochannel interference cancellation for multipath fading channels," *IEEE JSAC*, vol. SAC-11, No.7, Sept. 1993, pp.1067–75.

[12] M. Sawahashi *et al.*, "Pilot symbol-aided coherent multistage interference canceller using recursive channel estimation for DS-CDMA mobile radio," *IEICE Trans. Commun.*, vol. E79-B, Sept. 1996, pp. 1262–70.

[13] G. Tsoulos, M. Beach, and J. McGeehan, "Wireless personal communications for the 21st century: European technological advances in adaptive antennas," *IEEE Commun. Mag.*, vol. 35, Sept. 1997, pp. 102–9.

[14] S. Tanaka, M. Sawahashi, and F. Adachi, "Pilot symbol-assisted decision-directed coherent adaptive array diversity for DS-CDMA mobile radio reverse link," *IEICE Trans. Fundamentals*, vol. E80-A, Dec. 1997, pp. 2445–54.

[15] C. Berrou, A. Glavieux, and P. Thitimajshima, "Near Shannon limit error-correcting coding and decoding: Turbo-codes," *Proc. ICC '93*, Geneva, Switzerland, May 1993, pp. 1064–70.

[16] E. H. Dinan and B. Jabbari, "Spreading codes for direct sequence CDMA and wideband CDMA cellular networks," *IEEE Commun. Mag.*, this issue.

BIOGRAPHIES

FUMIYUKI ADACHI [SM '90] (adachi@mlab.yrp.nttdocomo.co.jp) received his B.S. and Dr.Eng. degrees in electrical engineering from Tohoku University, Sendai, Japan, in 1973 and 1984, respectively. In 1973 he joined the Electrical Communications Laboratories of Nippon Telegraph & Telephone Corporation (now NTT) and conducted various research projects related to digital cellular mobile communications. Since 1992 he has been with NTT Mobile Communications Network, Inc., where he is now a senior executive research engineer and director of the Wireless Access Laboratory. Currently he is leading a research group on wideband CDMA for IMT-2000. His research interests include: wideband/broadband CDMA, spreading code design, Rake and space diversity reception techniques, adaptive antenna array, and bandwidth efficient modulation and channel coding techniques. During the academic year 1984–1985, he was a United Kingdom SERC Visiting Research Fellow in the Department of Electrical Engineering and Electronics at Liverpool University. Since 1997 he has been a visiting professor at Nara Institute of Science and Technology, Japan. He has written chapters of three books: Y. Okumura and M. Shinji, Eds., *Fundamentals of Mobile Communications* (IEICE, 1986, in Japanese); M. Shinji, Ed., *Mobile Communications* (Maruzen, 1989, in Japanese); and M. Kuwabara, Ed., Digital Mobile Communications (Kagaku Shinbun-sha, 1992, in Japanese). He was a co-recipient of the *IEEE Vehicular Technology Transactions* best paper of the year award in 1980 and again in 1990.

MAMORU SAWAHASHI [M '88] received B.S. and M.S. degrees from Tokyo University in 1983 and 1985, respectively. In 1985 he joined NTT Laboratories, and in 1992 he transferred to NTT Mobile Communication Network, Inc. Since joining NTT, he has been engaged in the research of modem techniques for mobile radio communications, and code synchronization and interference cancellation techniques for DS-CDMA. He is now a senior research engineer with the an executive research engineer with the Wireless Access Laboratory. He is a member of the Institute of Electronics, Information, and Communication Engineers (IEICE) of Japan.

HIROHITO SUDA [M '82] received B.S. and M.S. degrees from Yokohama National University, Japan, in 1982 and 1984, respectively. In 1984 he joined the Electrical Communications Laboratories of NTT and conducted research related to digital speech transmission via cellular mobile radio. Since 1992 he has been with NTT Mobile Communications Network, Inc., where he is now an executive research engineer with the Wireless Access Laboratory. His studies lie in the area of channel coding for DS-CDMA. He is a member of the IEICE of Japan.